Chapter 2

Experimental Methodology

The present measurements were performed by using 14UD Bhabha Atomic Research Center- Tata Institute of Fundamental Research (BARC-TIFR) Pelletron accelerator at TIFR and Folded Tandem Ion Accelerator at Nuclear Physics Division, BARC, Mumbai, India. Proton beam of 22 MeV was used directly for the proton irradiations and $^{7}Li(p,n)$ reaction was used to generate neutrons of different end-point energies by varying the incident proton energy. In both proton and neutron irradiations, an activation method followed by the Off-line γ-ray spectroscopy technique was used. The details related to each of the stages and setup of the experiment are discussed in the present chapter.

2.1 Particle Accelerators

2.1.1 14UD Pelletron Accelerator

The 14UD Pelletron is a Tandem Van-de-Graff type electrostatic accelerator, which can accelerate any ion, having different charge states, from the lightest H-ion to a heavy Uranium [1] in the energy range up to a few hundred MeV depending upon the terminal voltage of the accelerator. The accelerator in Bhabha Atomic Research centre- Tata Institute of Fundamental Research (BARC-TIFR) facility is mounted in a vertical geometry within a stainless steel tank. A typical schematics of Pelletron setup is shown in Figure 2.1. The charged particle source (ion-source) is mounted at the top of the accelerator tower. A cesium sputter ion-source generates negative ions from a selected source, which are then accelerated to an energy up to $\approx$ 300 keV. These negatively charged particle accelerated at small energies are then injected to the main beam pipe of the pelletron through an injector magnet. The accelerator tank is insulated from the steel tank walls with SF_6, a highly insulating gas, commonly used to provide an insulation between two high voltage terminals. The SF_6 gas prevents the pelletron to be shorted with the wall of the tank. The beam is now accelerated towards the high positive potential terminal V_t, situated at the center of the tank, increasing the energy of the ions up to qV_t. The high electric potential at the terminal is achieved by a continuous transfer of charge to the terminal with the help of a continuously rotating chain of steel pellets. Inside the terminal, the ions are made to pass through a thin carbon foil or a small volume of a gas, known as stripper, where they loose electrons and become highly positive. Since, the terminal is at high positive potential, the positive ions now start to experience repulsion from the terminal, and hence, accelerate towards the bottom of the tank which is kept at the ground potential. Finally, the accelerated ion-beam can be switched to any of the beam-lines of interest present at the main beam hall of the BARC-TIFR facility with the help of switching magnets.

If the charge state of the positive ions, after passing through the stripper at the terminal is 'q', then the energy gained by ions during the acceleration to the base of the tank is qV_t. Therefore, the final energy of the ion beam can be given by,

$$E = E_0 + (q+1)V_t \tag{2.1}$$

Where, E_0 is the energy of ions accelerated from ion-source, q is the charge state after stripping.

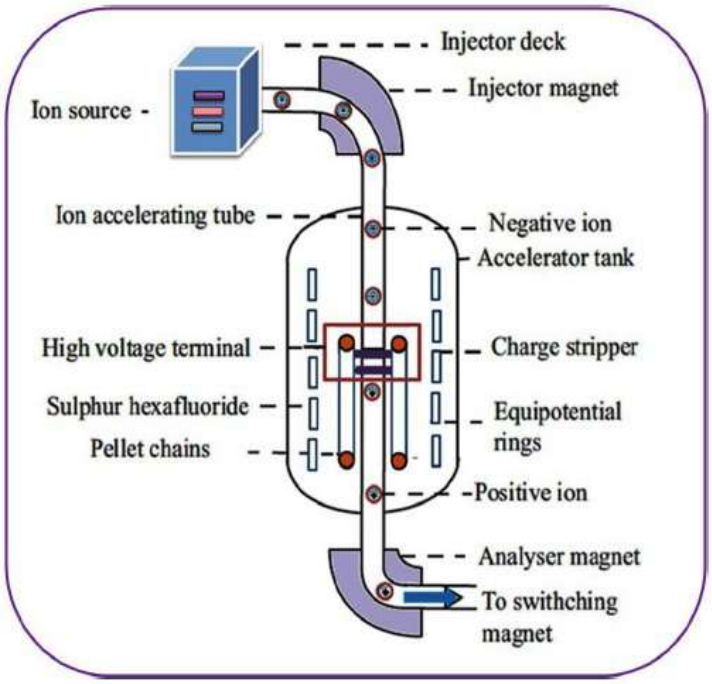

Figure 2.1: A schematic diagram of 14UD Pelletron Accelerator at BARC-TIFR Facility.

2.1.2 Folded Tandem Ion Accelerator (FOTIA)

The Folded Tandem Ion Accelerator (FOTIA) is situated at the Nuclear Physics Division of BARC, operates at the maximum terminal voltage of 6 MV. The beams of different ions can be accelerated using FOTIA. The accelerator was developed indigenously by BARC. In FOTIA, pre-accelerated negative-ion beam from the ion-source is injected into the accelerator using a magnet and an electrostatic deflector. The negatively charged ions are then accelerated towards the ion stripper, where a desired positive charge state of the ions can be achieved. The positively charged ions are now injected into a 180^o magnet inside high terminal voltage and bent into the high energy accelerating tube. The high accelerated beam can now be fed into the desired beam line using a magnetic steerer after 90^o analyzing magnet. The whole accelerator tube is kept at ultra high vacuum $\approx 10^{-8}$ Torr with a SF_6 gas assembly for insulation and to maintain high vacuum low temperatures around the high voltage terminal and 180^o magnet. A schematic diagram of FOTIA facility is shown in Figure 2.2.

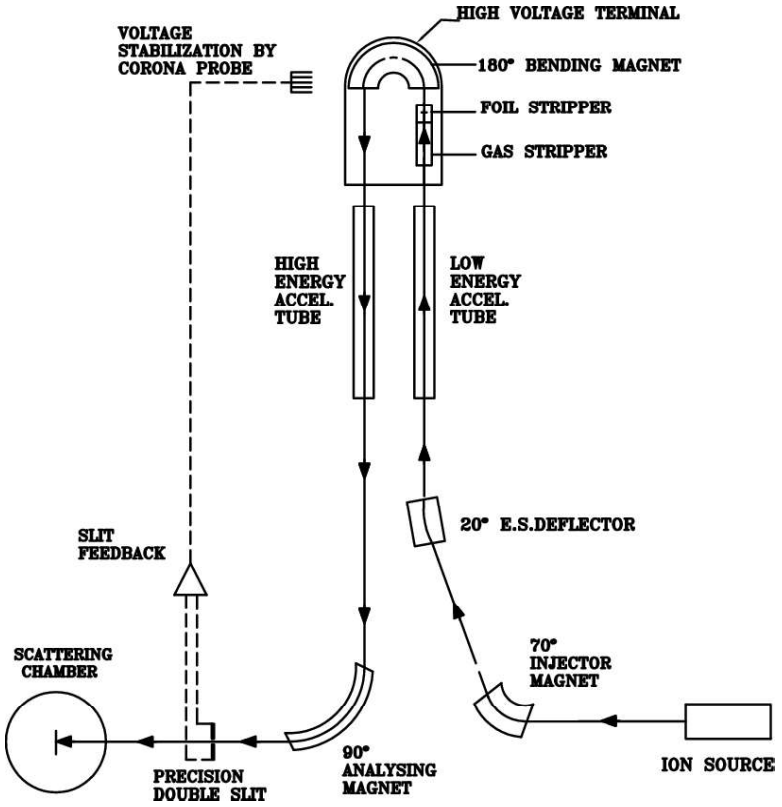

Figure 2.2: A schematic diagram of Folded Tandem Ion Accelerator (FOTIA) at Nuclear Physics Division, BARC.

In the present work, both the accelerators have been used extensively in order to get proton as well as neutron beams at different projectile energies. The Proton beam of 22 MeV was used at 14UD Pelletron for the study of proton induced reaction cross-sections at different projectile energies. The beam energy was reduced by using the stack foil technique. On the other hand, neutrons were generated by using $^{7}Li(p,n)$ reaction with 5 and 5.4 MeV protons from FOTIA and 8-22 MeV proton beams from Pelletron accelerator. A detailed discussion of the experimental setup for neutron and proton induced reactions are provided in sections 5.2 and 6.2, respectively.

2.2 Target Details

The target geometry is one of the important part of the activation analysis. In the present work, self supporting metal foils of natural occurring isotopes were used for the irradiation purposes in each experiment. The area of each target (sample) foil and corresponding monitor foil was taken as 1×1 cm^2, in order to avoid area corrections in neutron flux calculations. Each target was wrapped in thin aluminum (Al) foil ($\approx$ 0.0015 mm) to avoid

cross-contamination among the targets. Natural lithium (Li) foil was used to generate neutron beam by using $^{7}Li(p,n)$ reaction at 14UD Pelletron accelerator. On the other hand, natural lithium fluoride (^{nat}LiF) tablet was used for neutron production at FOTIA accelerator. The necessary target/monitor details which were used for the measurement of neuron-induced reaction cross-sections are given in Table 2.1.

For the proton induced reaction cross-section measurements, natural metal target foils were used. The proton beam energy was degraded along the stack of targets by using aluminum degraders. The area of targets as well as degraders were kept 1×1 cm^2 and separately wrapped in thin Al foil ($\approx$ 0.015mm) to avoid activity contamination and to collect the recoiling residues. The details of different targets which were used for the measurement of proton induced reaction cross-sections are given in Table 2.2.

2.3 Activation Technique

The activation of target simply refers to the interaction of projectile with the target nuclei. As a result of this interaction, a compound nucleus may form which possesses higher excitation states. The excited compound nucleus then decays to the lower excitation states by the emission of γ, n, p, β, or α-particles. The cross-section measurement technique may differ depending upon the type of particle one is looking during the de-excitation of the compound nucleus [2,3]. Depending upon this discussion, the activation techniques may be of two types, on-line or off-line. In on-line activation technique, the target is bombarded by using a specific beam of projectile nuclei and measure/record the outgoing γ, n, p, β, or α-particles during the irradiation process. However, in off-line activation, the measurement is usually carried out after the irradiation is over. In the present work, we have adopted the off-line activation technique [4,5] followed by the γ-ray spectroscopy by using a pre calibrated HPGe detector. The details regarding the target irradiation geometry are described separately for neutron and proton irradiations in the following subsections.

2.3.1 Neutron Activation

For the neutron irradiation experiments, a neutron-source is required together with a neutron-monitor. The neutron-source could be a natural source of neutrons or a reactor/accelerator based secondary neutron generator. Similarly, the monitoring of the neutron flux impinging on the target

Table 2.1: Target details for the n-induced reaction cross-section measurements.

Set.† No.	Samples		Incident E_P (MeV)	Area (cm^2)	Thickness (mm)	Weight (mg)
1.	Target/ Monitor*	^{232}Th	13	1×0.5	0.025	211.3
2.			16			201.1
3.			17			216.6
4.			21			246.8
1.	Target	^{nat}Mo	13	1×1	0.1	112.9
2.			16			104.0
3.			19			101.0
4.			22			107.2
1.	Monitor	^{27}Al	13	1×1	0.1	≈ 30.0
2.			16			
3.			19			
4.			22			
1.	Target	^{nat}Ni	5.4	1.1×1.2	0.025	127.4
2.			5	1.25×0.75		113.1
3.			8			
4.			16	1×1	0.1	≈ 22.0
5.			19			
1.	Monitor	$^{197}Au^a$	5.4	1.0×0.4	0.025	107.0
2.			5	1.1×0.7		138.7
3.		$^{27}Al^b$	8	1×1	0.1	≈ 30.0
4.			16			
5.			19			
3.		$^{115}In^c$	8	1×1	0.1	≈ 140.0
4.			16			
5.			19			

†here set represent targets with their corresponding monitors
*The ^{232}Th samples itself were used as the monitor by using the $^{232}Th(n,f)$ reaction [a]used as monitor at FOTIA for incident proton energies of 5.4 and 5 MeV
[b]used as monitor at Pelletron for incident proton energies of 8, 16 and 19 MeV
[c]used along side with ^{27}Al monitor at Pelletron

sample can be done by using a suitable reaction, detector or a direct time-of-flight (TOF) technique. The neutron-sources and monitor reactions which are used commonly worldwide are listed in Tables 2.3 and 2.4, respectively.

Table 2.2: Target details for the p-induced reaction cross-section measurements.

Set No.†	Target	Area (cm^2)	Thickness (μm)	Weight (mg)
1.	^{nat}Nb	1×1	22	≈ 22
2.	^{nat}Ag	1×1	32	≈ 31
3.	^{nat}Ti	1×1	12.7	≈ 5.5

†Each set was consisting of five target foils followed by Al degraders.

Table 2.3: List of some of the neutron generator reactions with their spectroscopic properties [10,11].

Reaction	Threshold (MeV)	Q-Value (MeV)	Neutron Energy (MeV)
(Fusion Based)			
D-D	-	3.268	2.5
T-T	-	11.33	0-9
D-T	-	17.58	14.1
(Charge Particle Induced)			(E_n Range)
$^3H(p,n)^3He$	1.018	-0.763	0.3-7.6
$^7Li(p,n)^7Be$	1.880	-1.644	0.12-0.6
$^9Be(p,n)^9B$	2.057	-1.852	*
$^9Be(d,n)^{10}B$	-	4.36	*
(Radioisotope Source)			(Avg E_n)
^{252}Cf			2.0
AmBe			4.2

Table 2.4: List of the commonly used neutron monitor reactions with their spectroscopic properties [11]

Reaction	Threshold (MeV)	Q-Value (MeV)	Cross-section (mb) at 14 MeV
$^{197}Au(n,\gamma)^{198}Au$	-	6.512	0.938
$^{115}In(n,n')^{115m}In$	-	-	≈ 3.0
$^{27}Al(n,\alpha)^{24}Na$	3.249	-3.132	≈ 120

In the present work, the neutrons were generated by using $^{nat}Li(p,n)$ reaction. In which, a proton beam of desired energy was taken from the Pelltron or FOTIA accelerator. A ^{nat}LiF tablet or a ^{nat}Li metal foil was used to generate the desired energy neutrons by varying the incident proton energy. The LiF tablet was wrapped in a thin Al and pasted on the front side of the target ladder, while the target (sample) foil together with the flux monitor foil are placed behind the Lif tablet at the back of the target ladder. Since Li is a highly reactive metal, therefore, the Li metal foil was sandwiched between two tantalum (Ta) foils of different thickness. Thick ta foil was used at the back of Li to stop the proton beam. Behind this Ta-Li-Ta stack, sample and monitor foils were kept together for the neutron irradiation. The stack was kept inside the 6 meter port for irradiation. A schematic diagram and a picture of the geometry of 6 meter port is shown in figure 2.3.

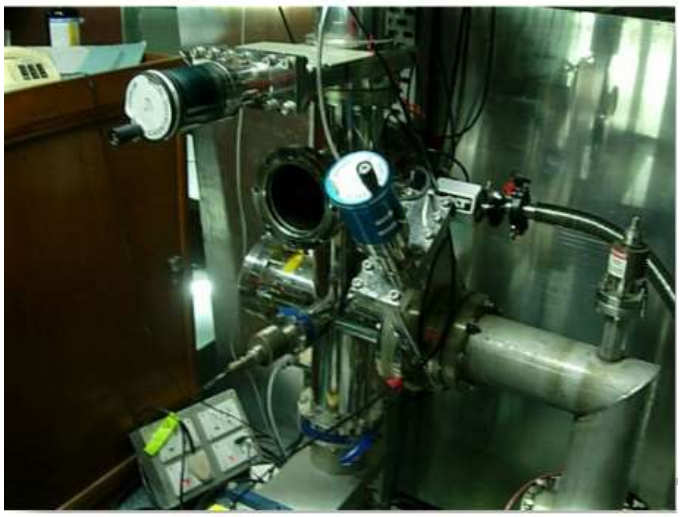

Figure 2.3: A pictorial view of the 6 meter irradiation setup at BARC-TIFR Pelletron accelerator.

2.3.2 Proton Activation

The proton irradiations were carried out at 14UD Pelletron accelerator by using stack foil activation technique. In this method, a stack of target-degrader foils is irradiated by 22 MeV proton beam. Each target foil is followed by an Al degrader foil of specific thickness to reduced the beam energy in steps of ≈2 MeV per target foil. The proton flux can be measured directly by the Faraday cup and/or by monitoring the beam current over

the period of the time of irradiation. The activity produced in the target foils after irradiation is used for the γ-ray spectroscopy. The 6 meter port as shown in Figure 2.3 was used for the proton beam irradiation of the target-degrader stack.

2.4 Off-line γ-ray Spectroscopic Technique

In order to measure the activities produced in the irradiated samples, we have used the off-line γ-ray spectroscopy method [6,7]. In this technique, the delayed γ-rays emerging from the samples are recorded using a pre-calibrated HPGe detector after the irradiation has been completed. This method sophisticates a user to record the γ-ray spectrum of the sample for a significant amount of time which helps in order to reduce the statistical uncertainty in the measurement. This technique also allows a user to count the samples repeatedly for a longer period of time according to the half-life ($T_{1/2}$) of residues under consideration. Despite of these advantages, the method is not suitable in order to measure the cross-sections of reaction residues which possesses a comparatively shorter half-lives of the order of a few seconds. Complete details regarding the HPGe detector used in the present work are given as follows.

2.4.1 High Purity Germanium Detectors

High Purity Germanium (HPGe) detectors are widely used semiconductor detectors for the on-line/off-line γ-ray spectroscopy in experimental nuclear physics, as well as in X-ray spectroscopy [8]. In solid state detectors,, when radiation passes the active volume of the crystal, it creates a number of electron-hole pairs along it's track. These generated charges are collected by applying an electric field across the crystal. Due to thermal excitation of atoms, a huge current flows in forward bias. However, in case of a reverse biased junction, the current flowing through the semiconductor is negligible and the current due to the ionizing radiation can be detected. Since the thickness of the depletion region is larger in reverse bias, therefore, semiconductor detectors are generally used in reverse bias. A schematic diagram of a HPGe detector is shown in Figure 2.4 [9]. A germanium detector can have a large depleted sensitive volume and therefore can be used as a detector to completely absorb γ-rays up to a few MeV. These detectors are called high-purity germanium detectors (HPGe) or hyper-pure germanium detectors as the impurities in the crystal are removed by using purification techniques. Impurities trap electrons and holes in the crystal and effect the performance of the detector. Consequently, germanium

crystals also doped with lithium ions (Ge(Li)), in order to produce an intrinsic region which helps electrons and holes to reach the contacts and to produce a signal.

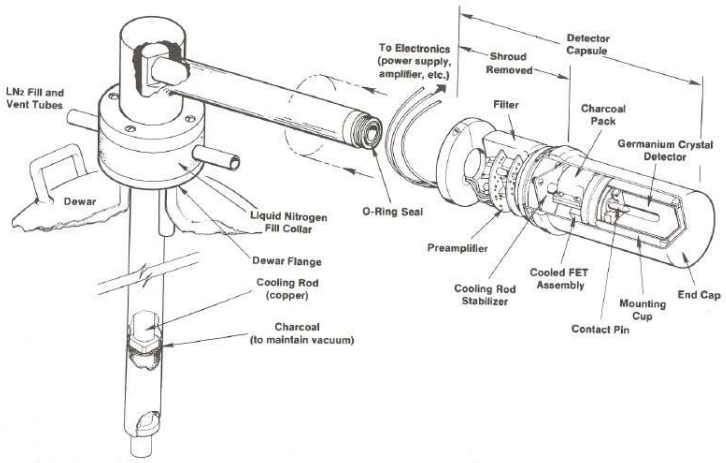

Figure 2.4: Schematics of a typical HPGe detector connected to a cooling dewar [9]

2.4.2 Energy Calibration and Resolution of the Detector

In the present work, each HPGe detector was calibrated using a ^{152}Eu source of known strength. The ^{152}Eu source [11] may decay by emission of various intense and well resolved γ–rays having the energies from 122 keV to about 1408 keV. The prominent γ-rays that are utilized in the calibration of detector along with their intensities are listed in Table 2.5 and characteristic γ-ray energy spectrum of ^{152}Eu observed is displayed in Figure 2.5.

The resolution of both the HPGe detector systems[1] were measured to be $\approx$ 1.8 keV for 1332 keV γ-ray of ^{60}Co. The HPGE detectors were coupled with a PC through a CAMAC based 4096 multichannel analyzer. Various γ-ray acquisition softwares like, MAESTRO [12], Genie [13] and FitzPeaks [14] were used for the recording and analysis of different spectra.

2.4.3 Efficiency of the Detector

The efficiency of the HPGe detector is determined by using the ^{152}Eu source [11]. The variation of efficiency with γ-ray energy for detectors is geometry independent, however, their absolute value depends on the detector geometry and is given by,

[1]One at FOTIA and another at Pelletron setup.

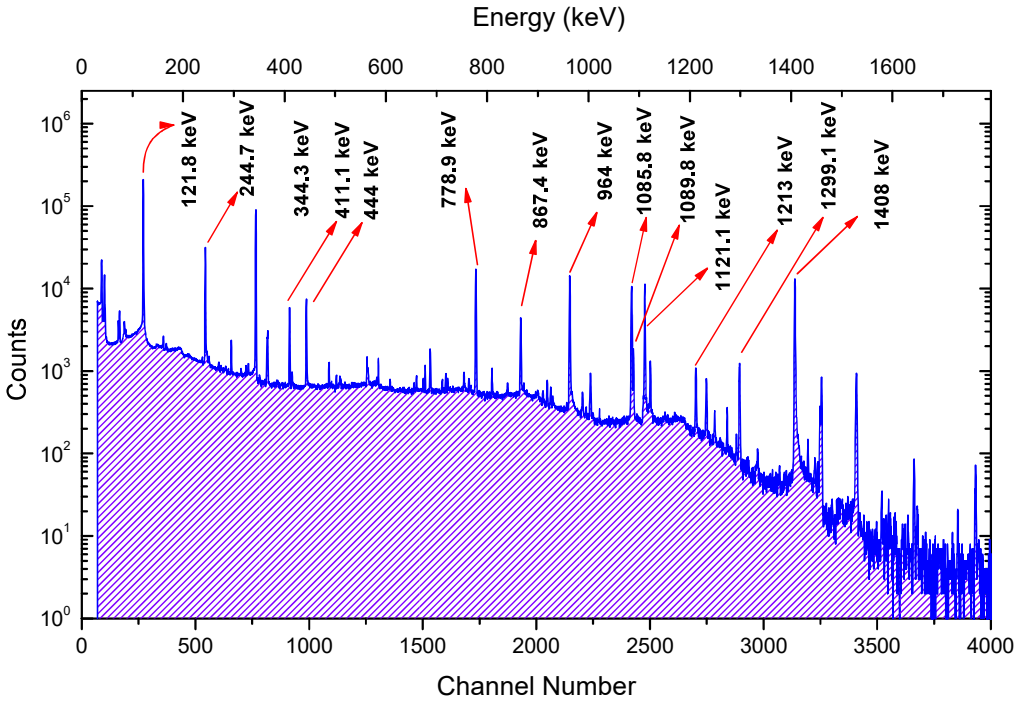

Figure 2.5: A typical recorded spectrum of a standard ^{152}Eu γ-ray source marked with prominent γ-lines

Table 2.5: γ-rays along with their absolute intensities (%) for the ^{152}Eu source

S. No.	γ-ray Energy (keV)	Absolute Intensity $(I_\gamma(\%))$
1	121.8	28.6
2	244.7	7.6
3	344.3	26.5
4	411.1	2.2
5	444.0	2.8
6	778.9	12.9
7	867.4	4.2
8	964.1	14.2
9	1085.9	10.2
10	1089.7	1.7
11	1112.1	13.6
12	1213.0	1.4
13	1299.1	1.6
14	1408.0	21.0

$$\varepsilon_G = K_c \frac{C}{N_0 I_\gamma e^{-\lambda T} \triangle t} \tag{2.2}$$

where, C is the observed counts of the γ-line of interest in $\triangle t$ time interval, N_0 is the disintegration rate of ^{152}Eu γ-ray at the time of production of the source, λ is the decay constant, T is the time interval between the dates of production and observation, I_γ is the absolute intensity [11] of the particular γ-ray and K_c is the correction factor for the coincidence-summing effect [15]. The coincidence summing correction was performed using the EFFTRAN code [16].

The source-detector arrangement which was used for the γ-ray counting measurement at 14UD Pelletron facility is shown in Figure 2.6.

Figure 2.6: Pictorial view of typical source-detector counting setup at BARC-TIFR Pelletron facility

The typical geometry dependent efficiency (ε_G) as a function of γ-ray energies (E_γ) for FOTIA as well as for Pelletron experiments at different distances from the detector end cap are shown in Figure 2.7. The efficiencies which are used for the analysis of the $^{232}Th(n,\gamma)$ reaction cross-sections are shown in Figure 2.7 (a), for the $^{100}Mo(n,2n)$ and $^{58}Ni(n,p)$,^{58} $Ni(n,2n)$ reaction cross-sections are shown in Figure 2.7 (b) and (c), whereas, the efficiencies used for the proton induced reactions are presented in Figure 2.7 (d).

A polynomial of degree four was found to be the best fit for these curves and can be written as,

$$G = aE_0 + bE_1 + cE_2 + dE_3 + eE_4 \tag{2.3}$$

Where a, b, c, d, and e are the constants depending on the source-detector distances and can be determined by the least square fit and E is the energy of the characteristic γ-ray.

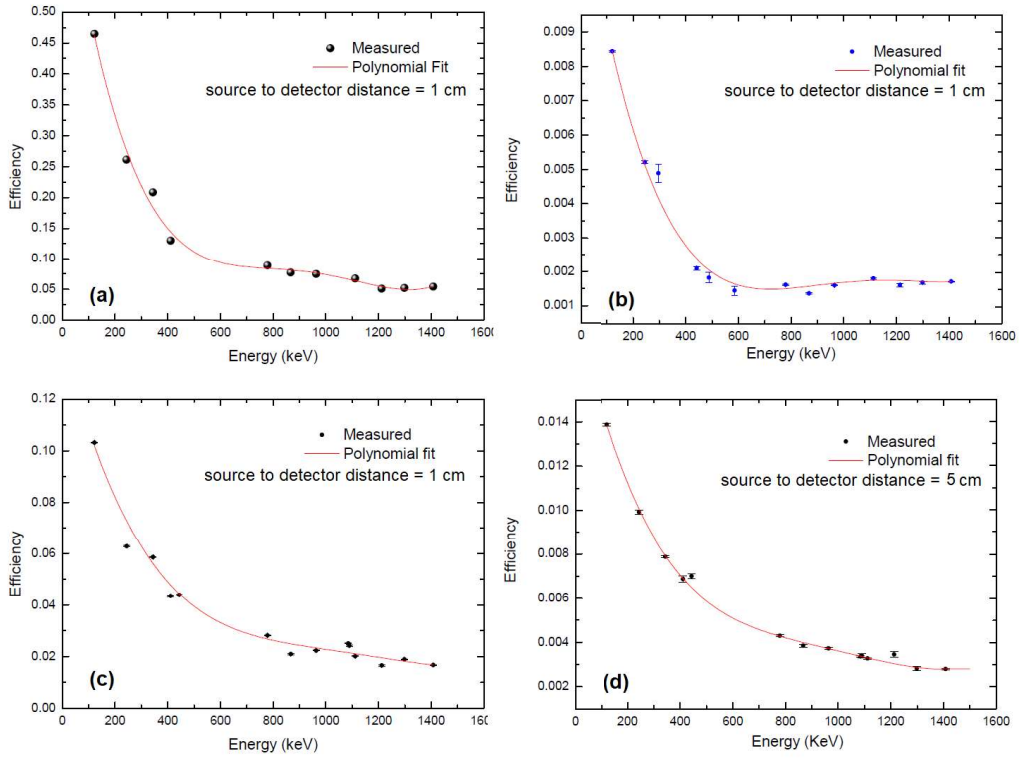

Figure 2.7: Measured efficiencies for the detector used for (a) the $^{232}Th(n,\gamma)$ reaction at BARC, (b) $^{58}Ni(n,p)$ reaction at FOTIA, BARC, (c) $^{58}Ni(n,2n)$ and $^{100}Mo(n,2n)$ reactions at TIFR and (d) for p-induced reaction measurements at TIFR at the 5 cm source to detector distance

2.5 Identification of the Reaction Residues

Each residue populated as a result of the interaction of projectile with target nucleus has a unique decay mode and γ-line. During the de-excitation, the formed residue emits characteristic γ-rays, which can be recorded by using a suitable detector. And hence, a specific residue can be identified by its characteristic γ-ray energies and branching ratios as the basic information [11]. The induced γ-ray activity in each target foil has been counted over a longer period of time following the half-lives ($T_{1/2}$) of the residues under consideration. In case of intermixing of γ-rays due to different isotopes, the contribution of each residue can be separated out by recording the induced activity for a considerably longer time [3]. The spectroscopic properties like; half-life, characteristic γ-ray, branching ratio and spin for the identified reside were taken from NuDat [11].

The general details regarding the experimental method and steps are provided in the present chapter. Specific details with a rigorous discussion about the neutron production and the stacks used in neutron and

proton activation are provided in the subsections 5.2 and 6.2, respectively, followed by the complete discussion on the measurement of the reaction cross-sections.

✠ ✠ ✠ ✠

Bibliography

[1] D. Kanjilal, S. Chopra, M. M. Narayanan, I. S. Iyer, V. Jha, R. Joshi, and S.K. Datta,*Nucl. Instr. and Meth A **328** (1993) 97.*

[2] E.V. Sayre, *Ann. Rev. Nucl. Sci., **13** (1963) 145.*

[3] R.C. Kotch, Activation Analysis Hand Book, Academic Press, New York and London, (1960).

[4] E. Gadioli et al, Nuclear Science Research Conference Series, Vol. **12**, eds. Z. Wilhelmi and G. Szeflinska, Harwood Academic, London, (1987).

[5] D.J. Parker et al., in proceeding of the 5th Intern. Conf. on Nuclear Reaction Mechanism, ed. E. Gadioli, Ricerca Scientifica de Educazione Permanente, Suppl. **66** (Milano, 1988).

[6] S. Mukherjee, B. Bindu Kumar, M. H. Rashid, and S. N. Chintalapudi, *Phys. Rev. C* **55** (1997) 2556 .

[7] J. Acharya, S. Mukherjee, G. F. Steyn, N. L. Singh, and A. Chatterjee *Phys. Rev. C* **93**, (2016) 024608 .

[8] G.F. Knoll, Radiation Detection and Measurement 3 rd edition (**Chapters 12 and 13**), John Wiley & Sons, (1999).

[9] HPGe Detector Manufacturing, ORTEC, `http://www.ortec-online.com`.

[10] Qtool: calculation of reaction Q-values and threshold, Los Alamos National Library, `http://cdfe.sinp.msu.ru/services/calc_thr/calc_thr.html`.

[11] NuDat 2.7β 2011, *National Nuclear Data Center, Brookhaven National Laboratory*, `http://www.nndc.bnl.gov/`.

[12] MAESTRO Multichannel Analyzer Emulation Software, ORTEC, `https://www.ortec-online.com/products/application-software/maestro-mca`

[13] Genie 2000 Gamma Analysis Software, MIRION Technologies, https://www.mirion.com/products/genie-2000-gamma-analysis-software.

[14] FitzPeaks Gamma Analysis and Calibration Software, Jim Fitzgerald, JF Computing Services, STANFORD IN THE VALE, Oxfordshire, SN78LE, https://www.jimfitz.co.uk/fitzpeak.htm.

[15] Thomas M. Semkow, Ghazala Mehmood, Pravin P. Parekh, Mark Virgil, Nucl. Inst. and Meth. in Phys. Res. A **290**, 2, (1990), 437.

[16] T. Vidmar, G. Kanish, G. Vidmar, Appl. Rad. Isot., **69** (2011), 908.